A NUMERICAL STUDY OF METAL PAD ROLLING INSTABILITY IN A SIMPLIFIED HALL-HÉROULT CELL

R. Gutt[1], V. Nandana[2] and U. Janoske[3]

[1] University Wuppertal, Gaußstr. 20, 42119 Wuppertal,
rgutt@uni-wuppertal.de

[2] University Wuppertal, Gaußstr. 20, 42119 Wuppertal,
nandana@uni-wuppertal.de

[3] University Wuppertal, Gaußstr. 20, 42119 Wuppertal,
uwe.janoske@uni-wuppertal.de

Key words: Magnetohydrodynamics, Volume of Fluid, Hall-Héroult process, OpenFOAM®

Abstract. Liquid metal instabilities in the aluminium production using the Hall-Héroult process are a known problem. During the production process, currents up to 800kA and voltages up to 5V are reached. The induced magnetic field from the current carrying busbars, especially the vertical component, creates in combination with the horizontal component of the current a high Lorentz force. This force induces liquid metal instability known as Metal Pad Rolling (MPR). Experimental investigations of MPR are rare, since cryolite dissolves most materials in short time, which make measurements inside the Hall-Héroult cell complicated. For this reason numerical simulations are needed to examine the flow- and the electromagnetic field, such that the stability conditions for Hall-Héroult cell can be predicted.

This work focuses on the development of a multi-phase/region solver to predict MPR instabilities. The solver is implemented in the open source framework OpenFOAM®. Volume of fluid method with phase-fraction based reconstruction approach is used to solve the multi-phase system. The magnetic field is implemented using the magnetic potential approach. The four step projection method [1] is employed to obtain a conservative formulation for the current density. A parameter study investigating the MPR in a simplified Hall-Héroult cell is carried out for a wide range of magnetic fields and current densities. One result of this study is that recalculating the magnetic field does not influence the maximum amplitude of the moving interface. For the current densities of $5\,kAm^{-2}$ and $6\,kAm^{-2}$, an increase in the external magnetic field initially destabilizes the Hall-Héroult cell, followed by restabilization. Further increase in the external magnetic field results in stronger instabilities based on simulations. Presumably, it is the first known occasion this specific behavior is observed in a numerical simulation. The frequencies of the MPR instability obtained from the simulation corresponds with the analytically determined frequency. Furthermore, a sensitivity study has been conducted to understand the influence of the solver specific parameters.

1 INTRODUCTION

The rotation period of newly born neutron stars, the movement of the liquid outer core of the earth and the sloshing interface of aluminium and cryolite in a Hall-Héroult cell have one thing in common, they are all magnetohydrodynamic (MHD) phenomena. MHD is a relatively new discipline. The term was firstly used by Alfvén [2] who investigated the propagation velocity (Alfvén velocity) of hydromagnetic waves in plasma with high magnetic fields. The main intention of MHD is to combine the discipline of fluid dynamics and the discipline of electromagnetics to describe the effect of moving conducting fluids on the electromagnetic fields and vice versa. Nowadays MHD related research plays an important role for many engineering applications such as an electrical storage using liquid metal batteries [3, 4, 5] and in the aluminium reduction using the Hall-Héroult process [6, 7, 8, 9]. A common problem of these applications are liquid metal instabilities.
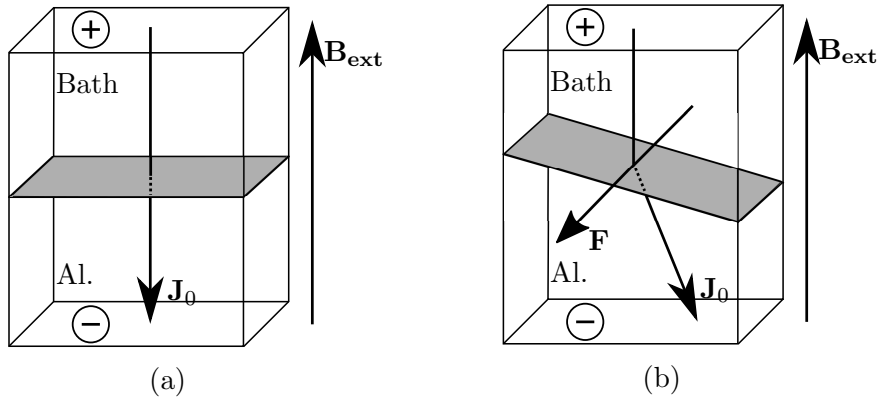
Figure 1: Simplified illustration of a Hall-Héroult cell. (a) Undisturbed interface with purely vertical current density. (b) Disturbed interface with horizontal current component.

This research work only considers the metal pad rolling (MPR) instability and focuses on a simplified Hall-Héroult cell as an application. Metal pad rolling, also called sloshing is a liquid metal instability, which only occurs in multi-phase systems such as liquid metal batteries and the Hall-Héroult process.

In an industrial Hall-Héroult cell the current goes through horizontal busbars into the anode and after passing the cell from the cathode into horizontal busbars again. The current going through the busbars will apply a toroidal magnetic field with a vertical component pointing in the opposite direction as the current flow. This external magnetic field is the main reason for the occurrence of the MPR [10]. For an undisturbed interface, illustrated in fig. 1a, between the cryolite and the aluminium, the current density is purely vertical and the Lorentz force induced by the cross product of the current density and the external magnetic field is zero. However, in a real cell the interface will never be perfectly horizontal due to external factors, which leads to a current density with a horizontal vector component. This component forms with the external magnetic field a Lorentz force perpendicular to both the current and the magnetic field which is shown

in fig. 1b. Since the conductivity of cryolite is much lower than the conductivity of aluminium, the current will take the path with the lowest resistance through the cryolite, which leads to a higher current density at the crest of the interface. A higher current in this context leads to a higher voltage at the crest. The horizontal current density is therefore always directed from the crest of the interface to the trough.

Looking from the top on fig. 1b the Lorentz force will rotate anticlockwise. The frequency of the oscillation can be analytically calculated by the solution of the gravity wave, which is given for a hexahedron with infinite height as [11],

$$\omega_{k,l} = \sqrt{\mathbf{g}\frac{(\rho_1 - \rho_2)\sqrt{k^2 + l^2}}{\rho_1 coth(\sqrt{k^2 + l^2}h_1) + \rho_2 coth(\sqrt{k^2 + l^2}h_2)}}. \tag{1}$$

Here k and l are the wave numbers defined by the corresponding modes m, n, respectively, the horizontal edge length L_y, L_z, as $k = m\pi/L_y$ and $l = n\pi/L_z$, respectively, the thickness of the aluminium layer h_1, the thickness of the cryolite layer h_2 and the densities of aluminium and cryolite ρ_1, ρ_2, respectively. For the MPR instability, the dominating mode is $m = 1$. For certain magnetic fields or current densities the mode 1 frequency is not enough to describe the interfacial movement and it is necessary to use higher modes. This analytical solution does not include the effect from the Lorentz force, which means this solution acts only as an approximation. The true angular frequency might differ.

A disturbed interface does not necessarily lead to the onset of the MPR instability. An onset criterion is given by Sele [12, 13] who compared the pressure induced by the Lorentz force with the pressure given by the gravitational force.

$$\beta = \frac{\mathbf{I}_0\mathbf{B}_{ext}}{h_1 h_2 \mathbf{g}(\rho_1 - \rho_2)} < \beta_{crit} \tag{2}$$

The field $\mathbf{I}_0$ is the current for the undisturbed Hall-Héroult cell and $\mathbf{g}$ is the gravitational acceleration. The Hall-Héroult cell, is stable if β is bellow the empirical determined critical value β_{crit}, which lies for an industrial Hall-Héroult cell in the range of $6 \leq \beta \leq 340$ [14].

Simulations are needed to examine the flow and the electromagnetic field, through which stability condition of the cell can be predicted. To achieve this, a numerical model to describe the MHD phenomena is developed in the open source framework OpenFOAM®. In addition a sensitivity and parameter studies for different external magnetic fields and current densities are carried out.

2   MATHEMATICAL MODELS AND IMPLEMENTATION

In this section the modeling of the MPR instability and the special treatment concerning the numerical implementation into the open source framework OpenFOAM® are described.

The behavior of an incompressible laminar fluid is described by the momentum equation as

$$\rho_0 \frac{\partial \mathbf{u}}{\partial t} + \rho_0 (\mathbf{u} \cdot \nabla)\mathbf{u} = -\nabla p + \mu \nabla^2 \mathbf{u} + \mathbf{f}, \tag{3}$$

where $\mathbf{u}$, μ, ρ_0, p and $\mathbf{f}$ are the velocity, the dynamic viscosity, the density, the pressure and the source terms, respectively. The source term $\mathbf{f}$ consists in this approach of the Lorentz force $\mathbf{f_L} = \mathbf{J} \times \mathbf{B}$, with $\mathbf{J}$ as the current density and $\mathbf{B}$ as the magnetic field and the gravitational force $\mathbf{f}_g = \mathbf{g}h\nabla\rho$, where h is the height and $\mathbf{g}$, the gravitational acceleration. The surface tension force is assumed to be negligible. In addition the conservation of mass must be fulfilled for the velocity field, which is given for incompressible fluids as

$$\nabla \cdot \mathbf{u} = 0. \tag{4}$$

The current density, is divided into a velocity dependent $\mathbf{j}$ and a velocity independent part $\mathbf{J_0}$

$$\mathbf{J} = \mathbf{J_0} + \mathbf{j} \tag{5}$$

and similarly for the electric potential,

$$\Phi = \Phi_0 + \phi. \tag{6}$$

The velocity independent current density is calculated as

$$\mathbf{J_0} = -\sigma\nabla\Phi_0, \tag{7}$$

where σ is the electric conductivity. For a system without free charges the electric potential is obtained with the requirement that the current density must be divergence free

$$\nabla \cdot (\sigma\nabla\Phi_0) = 0. \tag{8}$$

In the finite volume discretization, the fields are interpolated at the faces and the divergence is not solved for the center points of the control volumes. This means that conservation is ensured at the faces of the control volume. For the reconstruction of the current density to the center, a conservative interpolation scheme called four step projection method is used [1].

The velocity dependent current density is derived by applying Ohm's law for moving conductors,

$$\mathbf{j} = \sigma(-\nabla\phi + \mathbf{u} \times \mathbf{B}). \tag{9}$$

Since the current density must be divergence free the electric potential is obtained as

$$\nabla \cdot (\sigma\nabla\phi) = \nabla \cdot (\sigma(\mathbf{u} \times \mathbf{B})). \tag{10}$$

For the transport of the electric potential across different fluid-/solid-regions the current density of the connected regions needs to be equal at the sharing face, such that the following boundary condition can be derived

$$\Phi_b = \frac{\frac{\Phi_1\sigma_1}{\delta x_1} + \frac{\Phi_2\sigma_2}{\delta x_2}}{\frac{\sigma_1}{\delta x_1} + \frac{\sigma_2}{\delta x_2}}. \tag{11}$$

Here the indices b, 1 and 2 stand for the boundary and the two different regions, respectively, which are sharing the boundary.

Similar to the splitting of the current density and the electric potential into a velocity dependent and velocity independent part, the Lorentz force can be divided too,

$$\mathbf{f_L} = \mathbf{f_{L0}} + \mathbf{f_l}, \tag{12}$$

with

$$\mathbf{f_{L0}} = -\sigma(\nabla\Phi_0 \times \mathbf{B}), \tag{13}$$

$$\mathbf{f_l} = \sigma(-\nabla\phi + \mathbf{u} \times \mathbf{B}) \times \mathbf{B}. \tag{14}$$

In the momentum equation the velocity dependent force is now taken implicitly and the velocity independent force as an explicit source term. This treatment is used to reduce numerical fluctuation caused by strong body forces such as the Lorentz force and the pressure gradient [15].

To calculate the Lorentz force the magnetic field is needed. For the magnetic field the quasi static assumption is made, which means that the magnetic field is assumed to be time independent [3]. From Gauss' magnetism law it can be concluded that the magnetic field must be the rotation of a vector potential

$$\mathbf{B} = \nabla \times \mathbf{A}. \tag{15}$$

Together with Ampere's circuit law and by applying a Gauge transformation [16] the following formulation is obtained,

$$-\nabla^2\mathbf{A} = \mu_0\mathbf{J}. \tag{16}$$

To solve this equation suitable boundary conditions are needed. Those are derived by combining Gauss' magnetism law with Biot-Savarts' law

$$\mathbf{A}(\mathbf{r}) = \frac{\mu_0}{4\pi} \int_V \frac{\mathbf{J}(\mathbf{r}')}{|\mathbf{r} - \mathbf{r}'|} dV(\mathbf{r}'). \tag{17}$$

This volume integral is only solved at the boundaries by implementing a systolic algorithm which is known from astrophysics to calculate the gravitational force of multiple celestial objects on each other, which is the so called n-body problem. Another possibility to obtain the magnetic field is by solving Biot-Savart' law in the whole domain, which has the drawback that the time consumption is higher.

For the simulation of the two fluids, the volume of fluid method is used. In this method the momentum equation is only solved once for all fluids. A volumetric phase fraction α is introduced, to differentiate the different fluids. The phase fraction needs to be updated every time the fluid moves according to the momentum equation. Therefore the phase fraction is updated using the transport equation, which is given as,

$$\frac{\partial\alpha}{\partial t} + \nabla \cdot (\mathbf{u}\alpha) = 0. \tag{18}$$

The transport equation for the volume phase fraction is solved using MULES (Multidimensional Universal Limiter with Explicit Solution) [17].

A flowchart of the complete multi-phase/-region solver is given in fig. 2. For solving the electric potential over the different regions, a segregated approach is applied, using the boundary conditions given in eqn. 11. Another special feature of the solver is that the number of recalculations of the magnetic field is user defined. This means recalculation can be fully suspended to reduce the computational effort. For solving the momentum equation, the PIMPLE algorithm is used, where the outer most loop is residual controlled.
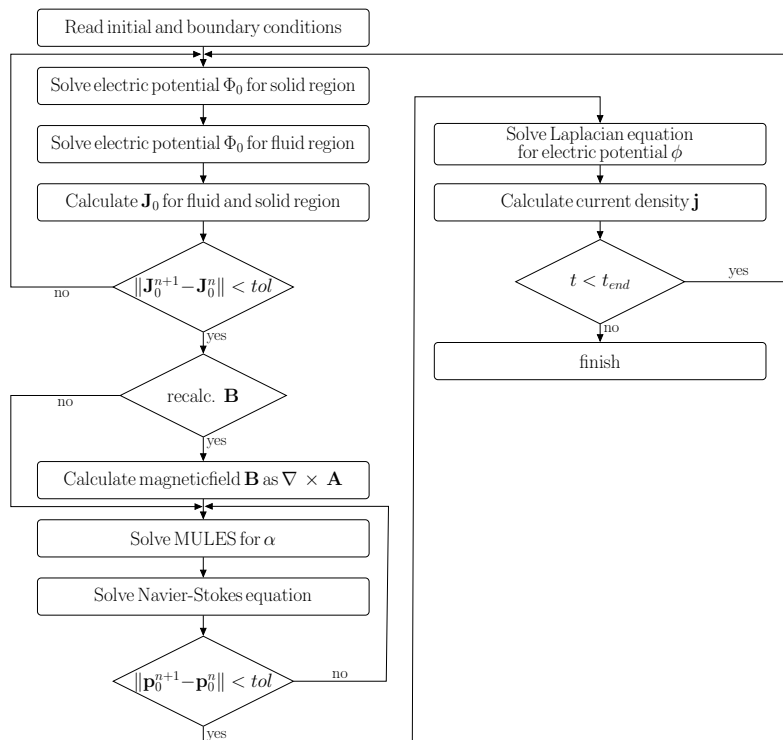
Figure 2: Flowchart of the multi-phase/-region solver using a segregated approach for solving over multiple regions.

3 RESULTS AND DISCUSSION

In this section the general case set-up for the multi-phase/-region solver is described in detail. Afterwards a sensitivity study is carried out for different cell width, Courant numbers and different numbers for recalculating the magnetic field. In addition the results of the parameter study are presented.

CASE SETUP

The multi-phase/-region case consists of three cuboidal shaped regions. The geometry is illustrated in fig. 3 with the corresponding edge lengths. At the top and at the bottom of

the geometry are the solid regions anode and cathode, respectively. In the fluid region aluminium is initialized at the lower half and cryolite is occupying the upper half of the region. For the external magnetic field a constant vector field is introduced, which points in the opposite direction of the gravitational acceleration.

The material properties of the aluminium and cryolite phase are as follows. For aluminium, the electric conductivity is given as $3.5 \cdot 10^6 \, Sm^{-1}$, the density, $2300 \, kgm^{-3}$ and the kinematic viscosity, $5.2 \cdot 10^{-7} \, m^2s^{-1}$. For cryolite, the electric conductivity is given as $2.5 \cdot 10^2 \, Sm^{-1}$, the density, $2150 \, kgm^{-3}$ and the kinematic viscosity, $1.18977 \cdot 10^{-6} \, m^2s^{-1}$.

The following boundary conditions are applied. The velocity and the gradient of the pressure are set to zero at the boundaries, which is congruent with the closed boundary assumption. The boundary conditions for the velocity dependent electric potential are set such that the potential at the top and the bottom of the fluid region are zero. The side walls are seen as insulated, which means the normal gradient of the electric potential is set to zero. The gradient of the potential is set according to the deliberated current density at the top of the anode. The gradient is calculated as

Figure 3: 3D view of the multiphase/-region geometry with the corresponding edge lengths. Including the regions anode (top), fluid (center) and cathode (bottom).

$$\nabla \Phi_0 = \frac{\mathbf{J}_0}{\sigma}. \tag{19}$$

At the cathode bottom, the potential is set to zero.

The divergence scheme of the momentum equation and the time discretization is done using a first order scheme. For all other discretization second order schemes are applied.

SENSITIVITY STUDY

A study of the solver specific parameter such as the influence of the mesh resolution and the time step is carried out. Before this is done, it is important to define the quantities which are comparable between the different simulations. The quantities of choice are the angular frequency and the amplitude of the oscillating interface. The analytical solution of the angular frequency is independent of the electromagnetic parameters (as shown in eqn. 1). However, it is a suitable quantity to compare different mesh resolutions and time steps. For the observation of the MHD effects, a quantity is needed which varies for different current densities and magnetic fields. For this reason the amplitude is chosen to compare multiple electromagnetic configurations. The benefit of the amplitude is that it shows significant changes for different Sele numbers. The drawback is that there is no

analytical solution to compare the obtained values from the simulation. For the sensitivity studies of the cell resolution and time step, the magnetic field is calculated only once. The error arising from this simplification is also investigated.

For different mesh sizes, the relative difference between the analytical and numerical results are shown in fig. 4a. An asymptotic behavior can be seen in fig. 4a, where the difference is less than 5% for cell width less than $3\,mm$. Since the analytical frequency does not take into account the electromagnetic fields, a minor difference between the frequencies obtained from the simulations and the analytical frequencies is expected. In fig. 4b the different cell widths are compared in terms of the amplitude of the oscillating interface. It can be seen that for a cell width above $2.5\,mm$ the amplitude is increasing monotonically. The decrease of the cell width below $2.5\,mm$, leads to an increase of the amplitude. The amplitude shows no clear convergence behavior for decreasing cell width. It is observed that the interface between aluminium and cryolite strongly diffuses for cell widths smaller than $2\,mm$. The diffusion is influencing the current density distribution, which is causing a destabilization of the system.
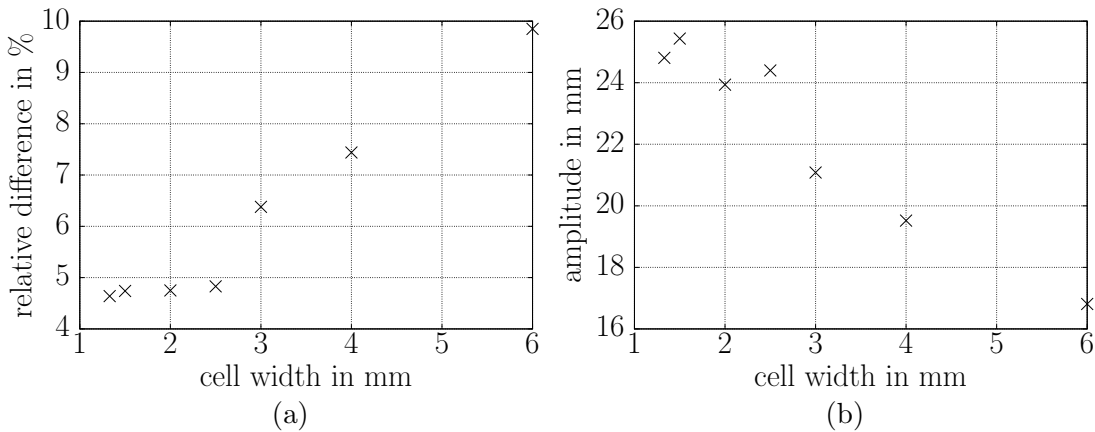
Figure 4: Relative difference of the angular frequency for different cell width (a). Plot of the amplitude over different cell widths (b). ($J_0 = 10\,kAm^{-2}$, $B_0 = 0.035\,T$)

A study of the influence of time step on the numerical simulation is done by limiting the maximum Courant number. For this study a cell width of $2\,mm$ is chosen, where the diffusion is reasonably limited and the angular frequency results are in a good agreement with the analytical solution. At first the relative differences of the angular frequency for different Courant numbers are compared to the analytical solution. As displayed in fig. 5a, the relative difference increases monotonically by decreasing the Courant number. This at first seems to be counter-intuitive, since the relative difference increases. Since the analytic solution is not taking into account the MHD effects, it can be concluded that the wave propagation is influenced by the Lorentz force. It can be seen that, the difference between the Courant number of 0.001 and 0.5 is less than 0.5%. As shown in fig. 5b, the amplitude is increasing monotonically for decreasing size of the Courant number. It can be assumed, that larger time steps are leading to a damping of the wave.

8
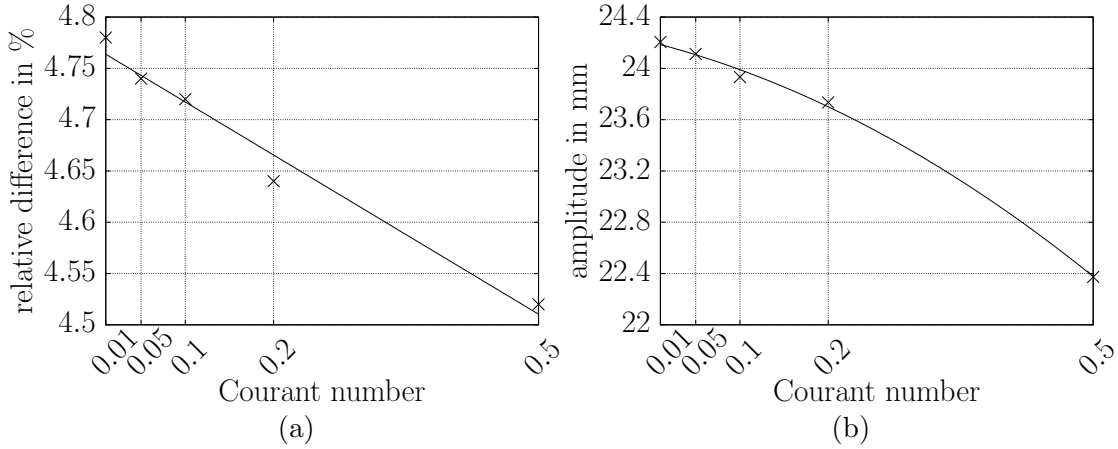
Figure 5: Relative difference of the angular frequency for different Co (a). Plot of the amplitude over different Co (b). ($J_0 = 10\,kAm^{-2}$, $B_0 = 0.035\,T$)

In the last step of the sensitivity study the influence of recalculating the magnetic field is investigated. Since the angle between the interface of the two phases and the horizontal is not negligibly small, it needs to be tested, if a recalculation of the magnetic field has an impact on the solution.

The simulations are carried out with a Courant number of 0.1 and a cell width of $3\,mm$. The cell width of $3\,mm$ is a compromise between accuracy and speed. The results of the study is displayed in fig. 6. The main difference between the plots is the time it takes to reach a stable oscillation. The difference between the different angular frequencies obtained from the simulations is less than $1\,\%$ and is therefore not shown here.
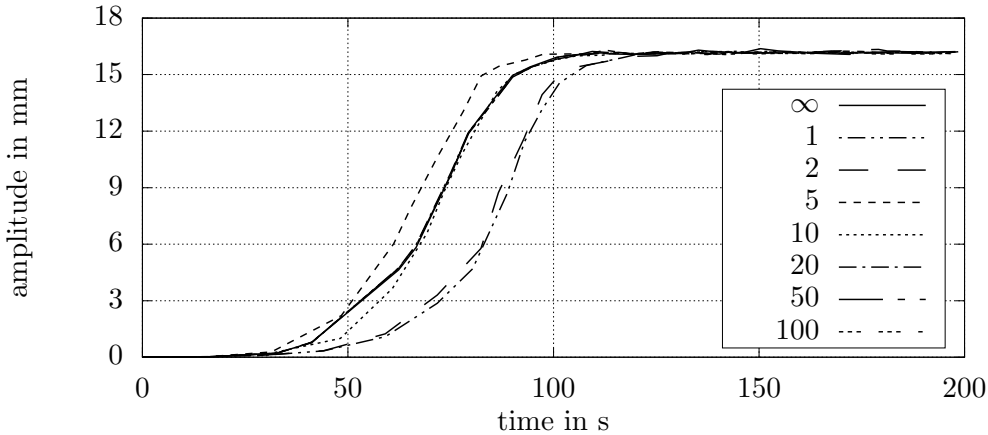
Figure 6: Maximum amplitude over time for a different number of recalculation iterations of the magnetic field **B**. ($J_0 = 10\,kAm^{-2}$, $B_0 = 0.035\,T$)

PARAMETER STUDY

For the parameter study multiple, combinations of the external magnetic field and the current density are applied. All simulations are carried out using a Courant number of 0.05 and a cell width of $2\,mm$. Figure 7a shows multiple plots of the maximum amplitude for different external magnetic fields, while the current density is held constant for each plot. For the current densities $8\,kAm^{-2}$ and $10\,kAm^{-2}$, the amplitude shows an asymptotic behavior for an increasing external magnetic field. For an external magnetic field larger $0.1\,T$, the fluid becomes strongly unstable. For the simulations where the current density is below $8\,kAm^{-2}$, the maximum amplitude firstly shows the same trend as the results for higher current densities, until the maximum amplitude reaches a point of inflection and eventually start to decrease for increasing magnetic field. For the current densities of $5\,kAm^{-2}$ and $6\,kAm^{-2}$, together with an external magnetic field of $0.15\,T$ the amplitude becomes stable again, a similar behavior has been also observed by the experimental study of Pedchenko et al. [7]. The amplitude in the experiment stagnated for increasing magnetic field strength and even decreased. It was claimed that this is due to the compensation of the Lorentz force. The magnetic field was not further increased in the experiment to observe whether a restabilization occurs.
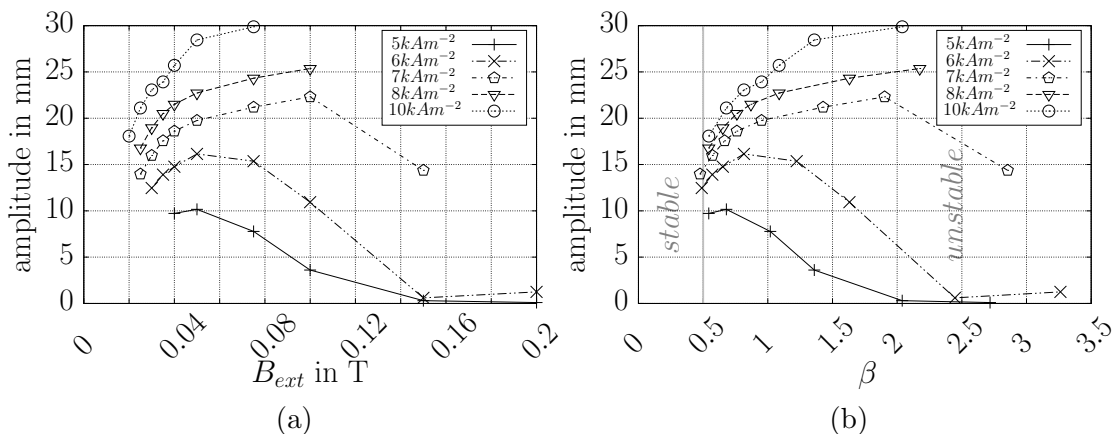
Figure 7: Maximum amplitude for different current densities and external magnetic fields (a). Maximum amplitude for different Sele values and external magnetic fields. The vertical gray line represents the critical Sele value (b).

This behavior is not yet fully understood and will be the topic of future works. By plotting the same values over the Sele values, instead of the magnetic field fig. 7b is obtained. The MPR instability for all current densities sets in for the same Sele value of $\beta_{crit} = 0.5$.

4   CONCLUSION

A solver has been developed and the first simulation results were carried out, which offer a good insight into the physics behind the MPR instability. It was shown that the

solver shows a good convergence behavior for different time steps, while the convergence behavior of the different mesh sizes needs to be addressed. In addition, it was shown that recalculating the magnetic field has no major impact on the maximum amplitude, which can reduce the computational cost in future studies. The obtained results from the parameter study needs to be investigated and will be the topic of further works.

5   ACKNOWLEDGEMENTS

REFERENCES

[1] Ni, M.-J. and Munipalli, R. and Morley, N.B. and Huang, P. and Abdou, M.A. *A current density conservative scheme for incompressible MHD flows at a low magnetic Reynolds number. Part I: On a rectangular collocated grid system.* Journal of Computational Physics, Vol. **227**, pp. 174–204, 2007.

[2] Alfvén, H., *On the cosmogony of the solar system.* Stockholms Observatoriums Annaler, Vol. **14**, pp. 2.1–2.33, 1942.

[3] Herreman, W. and Nore, C. and Cappanera, L. and Guermond, J.-L. *Tayler instability in liquid metal columns and liquid metal batteries.* Journal of Fluid Mechanics. Vol. **771**, pp. 79–114, 2015.

[4] Weber, N. and Beckstein, P. and Herreman, W. and Horstmann, G.M. and Nore, C. and Stefani, F. and Weier, T. *Sloshing instability and electrolyte layer rupture in liquid metal batteries.* Physics of Fluids, Vol. **29**, 2017.

[5] Zikanov, O. *Shallow water modeling of rolling pad instability in liquid metal batteries*, physics.flu-dyn, 2017.

[6] Flueck, M. and Janka, A. and Laurent, C. and Picasso, M. and Rappaz, J. and Steiner, G. *Some Mathematical and Numerical Aspects in Aluminum Production.* Journal of Scientific Computing, Vol. **43**, pp. 313–325, 2008.

[7] Pedchenko, A. and Molokov, S. and Priede, J. and Lukyanov, A. and Thomas, P.J. *Experimental model of the interfacial instability in aluminium reduction cells.* EPL (Europhysics Letters), Vol. **88**, 2009.

[8] Moreau, R.J. and Ziegler, D. *Stability of Aluminum Cells - A New Approach.* Springer International Publishing, Essential Readings in Light Metals, pp. 336–341, 2016.

[9] Steiner, G. *Simulation numérique de phénoménes MHD: application á l'électrolyse de l'aluminium.* EPFL (Lausanne), 2009.

[10] LaCamera, A.F. and Ziegler D.P. and Kozarek, R.L. *Magnetohydrodynamics in the Hall-Héroult process, an overview.* Light Metals, pp. 1179–1186, 1992.

[11] Denisova, I.V. *Problem of the motion of two viscous incompressible fluids separated by a closed free interface*, Acta Applicandae Mathematicae, pp. 31–40, 1994.

[12] Molokov, S. and El, G. and Lukyanov, A. *Classification of instability modes in a model of aluminium reduction cells with a uniform magnetic field.* Theoretical and Computational Fluid Dynamics, pp. 261–279, 2010.

[13] Sele, T. *Instabilities of the metal surface in electrolytic alumina reduction cells.* Metallurgical Transactions B, Vol. **8**, pp. 613–618, 1977.

[14] Gerbeau, J.-F. and Le Bris, C. and Lelièvre, T. *Mathematical Methods for the Magnetohydrodynamics of Liquid Metal.* Oxford University Press, 2006.

[15] Weber, N. and Galindo,V and Weier, T. and Stefani, F. Thomas Wondrak *Simulation of Instabilities in Liquid Metal Batteries.* Direct and Large-Eddy Simulation IX. ERCOFTAC Series, Vol. **20**. Springer, 2015

[16] Jackson, J.D. *Klassische Elektrodynamik.* de Gruyter, 2006.

[17] Deshpande, S.S. and Anumolu, L. and Trujillo, M.F. *Evaluating the performance of the two-phase flow solver interFoam.* Computational Science & Discovery, Vol. **5**, 2012.